# Kinetic Energy Release Distributions in the Dissociation of Energy-Selected Fluoroethene and 1,1-Difluoroethene Ions

**Felix Güthe,[†,‡] Robert Locht,[§] Bernard Leyh,[§] Helmut Baumgärtel,[†] and Karl-Michael Weitzel*,[†]**

*Institut für Physikalische und Theoretische Chemie, Freie Universität Berlin, Takustrasse 3, 14195 Berlin, Germany, and Département de Chimie Générale et de Chimie Physique, Bâtiment B6, Université de Liège, Sart-Tilman par 4000, Liège 1, Belgium*

The unimolecular dissociation of energy-selected fluoroethene and 1,1-difluoroetheneions has been investigated by the threshold photoelectron photoion coincidence (TPEPICO) technique. The breakdown diagrams of the 1,1-difluoroethene and fluoroethene have been recorded in the range 13−22 eV. From the time-of-flight spectra, complete distributions of the kinetic energy released (KERD) in the dissociation of these energy-selected ions have been derived. For the HF loss reaction channel, the KERD peaks at about 200 meV for low excitation energies but becomes thermal at higher excitation energies. For the F loss channel, the KERD peaks at zero kinetic energy for low excitation energy but at about 200 meV for high excitation energy. The analysis of the KERD provides evidence that consecutive fragmentation takes place for 1,1-difluoroethene at energies above 19 eV.

## I. Introduction

The photoelectron spectra (PES) of fluoroethene and 1,1-difluoroethene have been investigated extensively in the past, e.g., by Bralsford et al.,[1] Lake et al.,[2] and Turner et al.[3] Later these molecules have been investigated by Sell et al.[4] and Bieri et al.[5,6] In that work, assignments became possible on the basis of quantum mechanical calculations. Recently, the He(I) PES and the threshold PES (TPES) have been recorded at high resolution by Leyh et al.[7]

Chemical reactions of the fluoroethene cations have first been investigated by Lifshitz et al.[8,9] by means of electron impact ionization. Appearance energies have been derived, and possible mechanisms were discussed. Rate constants for some fragmentation reactions have been calculated by means of RRKM theory.[10]

The dissociative ionization of fluoroethene and 1,1-difluoroethene has first been studied by Reinke et al.[11,12] There, photoion yield curves have been recorded with a quadrupole mass spectrometer. A collection of the work on various fluoroethenes has been gathered by Kaufel.[13]

Ibuki et al.[14] have measured branching ratios of the fragments of 1,1-difluoroethene in the energy range 37−80 eV in a photoion−photoion coincidence (PIPICO) investigation. Photoelectron−photoion coincidence work (PEPICO) with a fixed wavelength (He(I)) and electron energy analysis has been performed for fluoroethene by Dannacher et al.[15] and for 1,1-difluoroethene by Frey.[16] Closely related to the work discussed here is the PEPICO investigation of Stadelmann and Vogt of the *cis-* and *trans-*1,2-difluoroethene.[17] In that work, metastable reactions and branching ratios have been observed.

A theoretical investigation of the three isomeric difluoroethene ions has been reported by Frenking et al.[18] In that work, several reaction channels of the difluoroethenes with the relevant intermediate energy minima and transition states were calculated.

The F loss reaction of the fluoroethene cation has been investigated in a theoretical paper by Roorda et al.[19] who discuss the possibility of an isolated state dissociation for the electronic C state at energies around 16.7 eV. They propose an avoided crossing between two reaction channels and predict the existence of one diabatic channel with high KER and one adiabatic channel with low KER. Momigny and Locht[20] later performed retarding field measurements to derive KER distributions for the $C_2H_3^+$ ion from fluoroethene, however, without energy selection of the parent ion. From a surprisal analysis, the authors derived a bimodal translational energy distribution which appeared to be in agreement with the assumption of an adiabatic and a diabatic reaction channel. For the 1,1-difluoroethene cation, Lorquet[21] suggested that the competition between $CF^+$ and $CH_2F^+$ formation is closely related to a late crossing of two potential energy curves.

The metastability of the HF loss and the corresponding KER of fluoroethene and 1,1-difluoroethene have been discovered by Jennings[22] and by Cooks et al.[23] with MIKES (metastable ion kinetic energy spectroscopy). In a more recent MIKES investigation, the KER of all fragments of 1,1-difluoroethene has been obtained by Franck.[24] Kim[25] analyzed the peak shape of the MIKES peak for the HF loss reaction and derived a KER distribution for the lifetime-selected sample in that experiment.

In this work, we describe the first investigation of the fluoroethene and the 1,1-difluoroethene ions by the threshold photoelectron photoion coincidence technique (TPEPICO). The aim of this work is to contribute to a better understanding of the energetics and the mechanism of the unimolecular decay reactions of these ions. This is achieved by analyzing complete kinetic energy release distributions (KERD) for energy-selected

* Corresponding author. E-mail: weitzel@chemie.fu-berlin.de.
† Freie Universität Berlin.
‡ Present address: Institut für Physikalische Chemie, Klingelbergstrasse 80, Universität Basel, CH-4056 Basel, Switzerland.
§ Université de Liège.

Kinetic Energy Release Distributions

*J. Phys. Chem. A, Vol. 103, No. 42, 1999* **8405**

ions. For many molecular ions, kinetic energy release distributions (KERD's) have been derived by the retarding field method. However, only very few examples of the KERD for energy-selected ions are known to date.

## II. Experimental Setup and Methods

The dissociation of fluoroethene and 1,1-difluoroethene ions has been investigated in the energy range between 13 and 22 eV by means of the threshold photoelectron photoion coincidence technique (TPEPICO).[26,27] The experimental setup has been described in previous publications.[28,29] Only a brief description will be given here. The measurements were performed in an effusive beam at room temperature. The molecules were ionized by radiation from the synchrotron radiation facility BESSY I in Berlin dispersed in the 3m NIM1 beamline. Energy selection of ions is achieved by detecting threshold photoelectrons and photoions in coincidence. The electron energy analyzer (steradiancy principle) is designed to transmit threshold electrons preferentially. The experiments discussed in this paper have been performed at an overall resolution of 20 meV (determined by the slits of the monochromator (200 $\mu$m) and the extraction field ($E_{acc}$) in the ionization region (40 V/cm)). The extraction field chosen in the experiment reflects a compromise between the desired mass resolution (which can be increased in a higher field) and the desired electron energy resolution (which can be increased in a smaller field). In particular, the extraction field had to be chosen high enough to achieve a mass resolution sufficient to separate the products of HF abstraction and F abstraction, both of which might be broadened by a large kinetic energy release (KER). For the analysis of the KER distributions, we preferred the extraction to take place in a static field. Besides from the energy resolution, a small acceleration field will also improve the sensitivity of the KER analysis. On the other hand, discrimination effects have to be considered in small fields.

The ions were analyzed in a Reflectron spectrometer, which has been optimized for the investigation of metastable reactions.[28,30] Time-of-flight (TOF) spectra were recorded by employing threshold electrons as a start and ions as a stop signal for a time to amplitude converter (TAC), thus enforcing the coincidence condition. From these TOF spectra, the fractional abundances were derived and plotted versus the excitation energy (photon energy) in a breakdown diagram.

**II.1. Simulation of the KERD.** In the following section, we briefly describe the simulations of ion time-of-flight distributions. In this work, the ion spectrometer is set up in a way that the time-of-flight distribution of any fragment ion signal is determined by the distribution of the KER in the reactions producing these fragments and by the kinetic energy of the neutral parent molecules due to the temperature of the sample. The peaks are in general broadened because ions that initially move away from the detector need some time to turn around in the electric field before being accelerated toward the detector. Ions that initially move in the opposite direction are detected earlier.

In the case of Gaussian peak shapes, the width of ion TOF distributions are in general translated into an average KER value according to a procedure described by Stockbauer.[31] However, Baer et al.[32] and later Powis et al.[33] have demonstrated, that it is possible to derive also complete KER distributions from the ion TOF distribution. The simulation of TOF distributions employed in this work differs in certain details such as taking into account discrimination effects and having a smaller step size.

To find out which KER distribution leads to the observed peak shape, one has to simulate the peak shape based on known
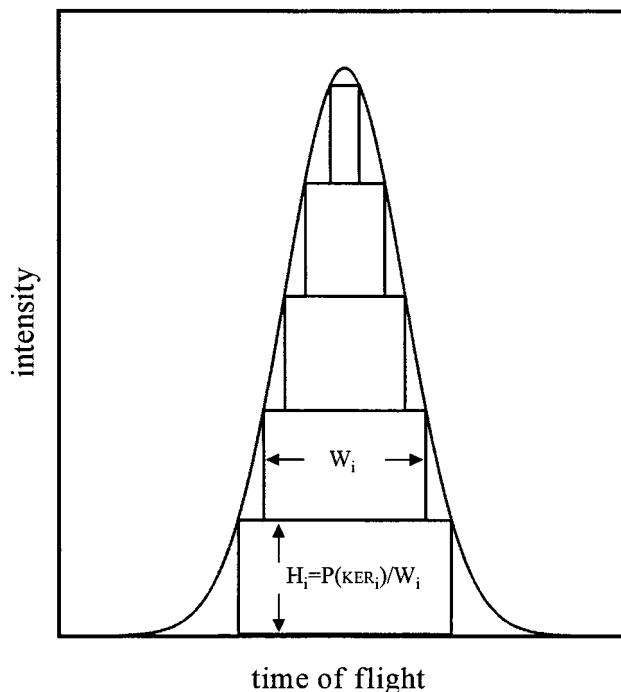


**Figure 1.** Schematic illustration of constructing a TOF peak with Gaussian shape by superposition of several rectangular functions of width $W_i$ (in time) and height $H_i$. $P(KER_i)$ is the probability of a particular $KER_i$.

parameters of the spectrometer and based on an analytical KER distribution which is then adjusted in order to achieve the best fit to the experimental spectrum. To exclude artifacts from the imaging properties of the spectrometer, the simulation is calibrated against TOF peaks of known systems, e.g., thermal argon. In general, the measured peak widths are 0−10% wider than the calculated peak widths. This effect is incorporated in the simulation procedure and is repeated for every spectrometer setting.

Reactions characterized by the release of a single kinetic energy lead to a rectangular peak of width $W$ in the time-of-flight spectrum[34,35] as shown in eq 1, where the kinetic energy of the daughter ion $KE_D$ is expressed as a function of $q$ (the charge of the ion), $W$ (the full width of the rectangular peak), and $M_D$ (the mass of the daughter ion). This equation holds true for translationally cold parent molecules. The possible effect of thermal kinetic energy of the parent will be discussed at a later point. $KE_D$ is connected to the total kinetic energy release of the reaction KER by laws of momentum and energy conservation[31] as shown in eq 2 ($M_P$ is the mass of the parent ion).

$$KE_D = \frac{1}{8}(qE_{acc})^2\left(\frac{W}{M_D}\right)^2 \qquad (1)$$

$$KER = KE_D\frac{M_P}{M_N} \qquad (2)$$

However, most chemical reactions are associated with a distribution of kinetic energy release rather than a single KER value. In that case, the total time-of-flight spectrum can be constructed by a superposition of many rectangular basis functions as indicated schematically in Figure 1. The weight $P(KER_i)$ with which each individual $KER_i$ contributes to the total KER distribution is then related to the height of the rectangle by $H_i = P(KER_i)/W_i$. In the present work, the number

of basis functions has been chosen as approximately half the number of points in the experimental TOF spectrum. In the simulation, the KERD is adjusted until the best agreement between simulation and experiment is obtained.

As mentioned earlier, a similar approach has been employed by Powis and co-workers[33] and Baer and co-workers.[32] One important difference is that the number of basis functions is significantly higher in this work. This leads to a better representation of the KERD's. Consequently, it was possible to employ analytical functions for the KERD from statistical theories.[36] More specifically, we used one distribution which has a maximum at zero KER and another one with a maximum different from zero. The former are in general relevant for narrow TOF peaks, the latter for broad TOF peaks. These distributions can also be shifted by a certain amount of energy. This is often necessary in order to simulate peaks with a flattened top. The maximum possible total KER is given by the difference between the photon energy and the appearance energy of the fragment. Beyond that energy, the KERD's are always cut off.

All experiments described in this work have been performed on thermal samples of the molecules. This thermal energy will affect the TOF distributions. Here, the thermal translational energy of the parent ions is taken into account explicitly by convoluting the KERD discussed above with the corresponding thermal energy distribution. However, this contribution is in general of minor importance. For reasons of comparison, the KERD's displayed in the result section do not contain the thermal energy, in other words they correspond to a 0 K sample.

It is well-known that the TOF peaks of ions which are characterized by a Maxwell–Boltzmann velocity distribution of translational energies (e.g., for a thermal sample of ions) have a Gaussian peak shape.[34] One critical test of the simulation is to check that a thermal KER distribution does in fact lead to a Gaussian TOF distribution, which is indeed the case in this work. Furthermore, the simulation of thermal noble gas spectra (no reaction) provides the calibration already mentioned above.

For high KER values, ions with high kinetic energy components perpendicular to the spectrometer axes may become discriminated, leading to a dip at the center of the ion TOF distributions. In the fluoroethene experiments, e.g., even for a total KER of 4 eV only 20% of the $C_2H_2^+$ fragment ions would become discriminated, at a total KER of 3 eV only 8%. For most of the experiments such high KER values are of minor importance. Because of the particular experimental conditions the discrimination was more severe for the difluoroethene. This discrimination has been taken into account explicitly in all the analysis presented in this work. It depends on the geometry of the spectrometer and the ionization region as well as the applied extraction fields. There are basically two ways to account for the discrimination, either by simulating ion trajectories[33] or by employing an appropriate transmission function. Both methods have been tested, but the effective transmission function turned out to be more convenient and equally precise. Although the transmission function might be critical for high KER, it is possible to model even KER distributions where discrimination is affecting the peak shape strongly. We note that even for high KER the edges of the ion TOF distribution are basically not affected under the current conditions.

The analysis of KER distributions presented here turned out to be very sensitive to low kinetic energies, because these energies give peak shapes with a narrow top. Flat topped peaks, on the other hand, can only be modeled by a distribution where low KER values do not contribute. The analysis is also very sensitive to the high-energy part of the distribution, because
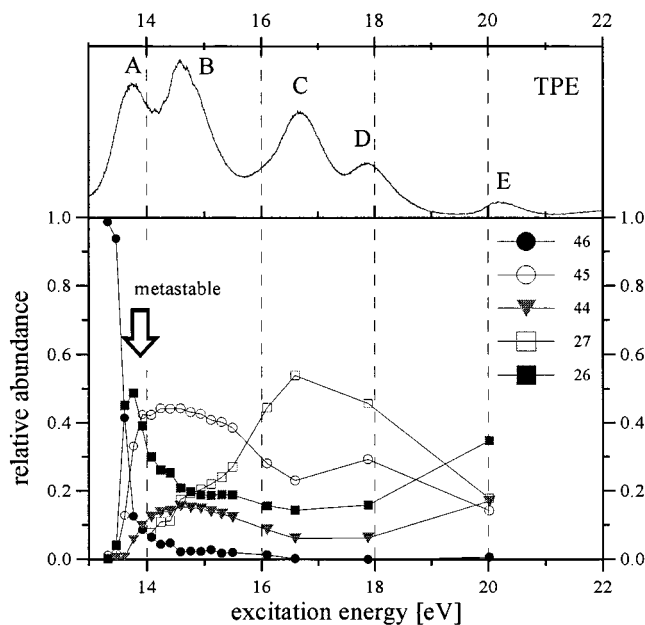


**Figure 2.** Lower part: breakdown curve of fluoroethene for the fragments with $m/z = 45$ ($C_2H_2F^+$), 44 ($C_2HF^+$), 27 ($C_2H_3^+$), 26 ($C_2H_2^+$), and the parent ion ($C_2H_3F^+$) in the energy range 13.5−20 eV. The arrow indicates the region where the reaction is metastable. Upper part: TPE spectrum of fluoroethene (bands are labeled A, B, C, D, and E) taken from ref 7.

only a few rectangular functions are broad enough to contribute to the far edge of the TOF peaks. However, since the $KER_i$ is proportional to the square of the $W_i$, it is clear that the absolute precision of the attained values is better for low KER's. From the KERD, an average value $\langle KER \rangle$ can be derived by averaging over all $KER_i$ in order to compare with other data, which only discuss this average value.

## III. Results and Discussion

In this contribution, the reactions of the fluoroethene ion and the 1,1-difluoroethene ion have been studied by recording coincidence TOF spectra in the range between 13 and 22 eV. The corresponding breakdown diagrams are shown in Figures 2 and 3. For comparison, the threshold photoelectron spectra (TPE) recorded by Hottmann et al.[7] are shown. These TPES's have been measured with a different spectrometer at higher resolution (ca. 5 meV). Both molecules have a distinct vibrational structure in the X state. The adiabatic ionization energies of fluoroethene and 1,1-difluoroethene are 10.36 and 10.30 eV,[7] respectively. In Figures 2 and 3, only the range between 13 and 22 eV relevant for the reactions under investigation is shown. In this region, the fluoroethene spectrum exhibits five electronic states with vertical ionization energies (estimated adiabatic IE's in parentheses) at 13.8 eV (13.2 eV) (A), 14.6 eV (14.3 eV) (B), 16.7 eV (15.6 eV) (C), 17.9 eV (17.5 eV) (D), and 20.2 eV (19.4 eV) (E). The spectrum of 1,1-difluoroethene exhibits five bands at 14.8 eV (14.1 eV) (A), 15.7 eV (15.5 eV) (B), 18.2 eV (17.8 eV) (C), 19.8 eV (19.2 eV) (D), and 21.5 eV (21.0 eV) (E). In the case of 1,1-difluoroethene, the higher electronic states also show a vibrational structure. This indicates that these states are relatively long lived and are not decaying instantaneously.

**III.1. Dissociation of Fluoroethene Ions.** In the range between 13 and 22 eV, the most abundant fragments are due to the loss of H ($m/z = 45$), $H_2$ ($m/z = 44$), F ($m/z = 27$), and HF ($m/z = 26$) from the parent ion ($m/z = 46$). The fractional
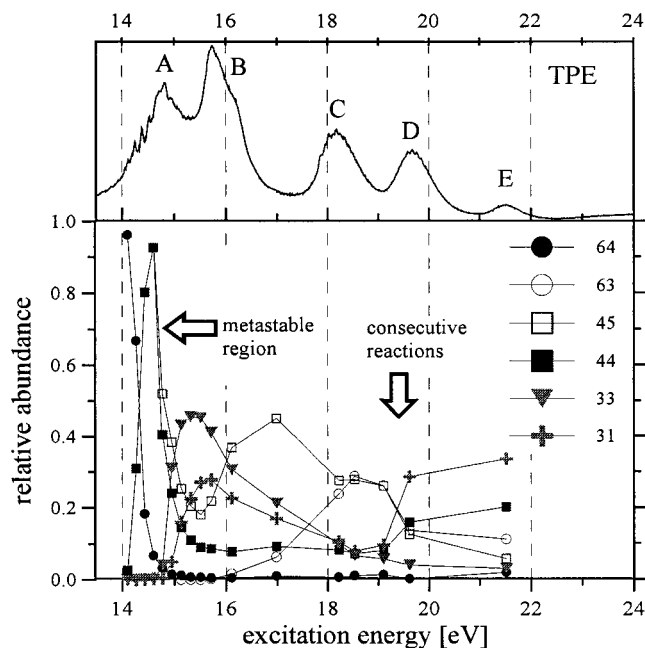
Kinetic Energy Release Distributions

*J. Phys. Chem. A, Vol. 103, No. 42, 1999* **8407**



**Figure 3.** Lower part: breakdown curve of 1,1-difluoroethene for the fragments with $m/z = 63$ ($C_2HF_2^+$), 45 ($C_2H_2F^+$), 44 ($C_2HF^+$), 33 (CFH$_2^+$), 31 (CF$^+$), and the parent ion ($C_2H_2F_2^+$), $m/z = 64$, in the energy range 13.5−22 eV. The arrows indicate the region where the reaction is metastable or where consecutive reactions are changing the fragmentation pattern strongly. Upper part: TPE spectrum of 1,1-difluoroethene (bands are labeled A, B, C, D, and E) taken from ref 7.

abundances of these ions have been derived from the intensities of the energy-selected TOF spectra and plotted into a breakdown diagram in Figure 2. Other fragments have been observed, but have a relative abundance of less than 4% up to 20 eV.[13] The appearance energies of these four ions lie all relatively close together and are all under 14 eV, as is summarized in Table 1. Also given are the thermochemical thresholds of the reactions, which have been calculated from Lias et al.[37] The appearance energies are well-known from Kaufel's work.[13] Therefore, we give only the values for the TOF spectrum for the lowest energy, where we observed this ion.

The first energetically accessible reaction channel is the HF abstraction (formation of $C_2H_2^+$, $m/z = 26$), which is metastable at the threshold. Our appearance energy is lower by about 100 meV than that of Kaufel,[13] which has been determined with a quadrupole mass spectrometer. This is due to the kinetic shift of this reaction, which is affecting the two experiments in a different way. This metastable reaction has been investigated in more detail in a different work.[30] The appearance potential is still lying more than 1 eV above the thermochemical threshold. This indicates that the reaction proceeds over a barrier.

The H loss reaction (formation of $C_2H_2F^+$, $m/z = 45$) is energetically the second lowest channel and has been observed at the thermochemical threshold. This reaction is also metastable at the threshold. In the Reflectron this reaction shows a clear signal for a metastable decay in the drift region.[30] Between 14 and 16 eV, the H loss is the most abundant reaction.

The H$_2$ loss reaction (formation of $C_2HF^+$, $m/z = 44$) can be clearly observed at an energy which lies about 120 meV below the expected thermochemical threshold. This cannot be explained by thermal energy or experimental uncertainty. From analyzing the thermochemistry of the species involved we conclude that the heat of formation for $C_2HF^+$ is 1181 kJ/mol instead of 1193 kJ/mol as reported in ref 37. Close to the threshold, the H$_2$ loss reaction is a 1,2-elimination (The

vinylidenic fragment is much higher in energy than the acetylenic fragment). Most likely, the reaction path includes a significant barrier. It is interesting that this barrier does not lead to a shift in the appearance energy. One reason for that could be a fast tunneling process of the H atoms through this barrier. The appearance energy of the F loss reaction (formation of $C_2H_3^+$, $m/z = 27$) is in the range, where the reaction is still metastable and the peak of the neighboring mass (HF loss) is asymmetrically distorted. This makes the identification of the peak difficult in this range. Therefore, this fragment is not explicitly drawn into the breakdown diagram in Figure 2 for energies below 14 eV. The relative abundance of the $C_2H_3^+$ ion is increasing and reaches a maximum at 15.5 eV. It is the most abundant species in the range between 16 and 18 eV. Some of the fragments listed in Table 1 are not significantly abundant in the energy range discussed here but are observed at 20.02 eV; for example, the mass 31 and 14 ions have a relative abundance of 3.7% and 4%, respectively, at 20.02 eV.

**III.2. Dissociation of 1,1-Difluoroethene Ions.** For the 1,1-difluoroethene, the most abundant fragments in the range under 20 eV excitation energy are the products of the H loss ($m/z = 63$), F loss ($m/z = 45$), and HF loss ($m/z = 44$) and the products of the CC bond cleavage $m/z = 31$ (loss of CH$_2$F) and $m/z = 33$ (loss of CF). The relative abundances for these fragments are shown in the breakdown diagram in Figure 3. At higher energies some other fragments can also be observed (Table 2). At 19.61 eV, three fragments not shown in the breakdown diagram are appearing with a fractional abundance of more than 4%: $m/z = 43$ (fractional abundance = ca. 4,1%), $m/z = 26$ (6.7% at 20.08 eV), and $m/z = 14$ (16.9% at 20.08 eV). In our experiment none of these ions appear at energies below 17.78 eV.

The energetically lowest reaction channel is again the HF abstraction (formation of $C_2HF^+$, $m/z = 44$) which can be observed at an energy of 14.10 eV. This is about 80 meV below the value of Kaufel and is due to kinetic shift. The thermochemical threshold for this reaction is about 1.1 eV lower, indicating a significant barrier along the reaction path. The threshold for forming the vinylidene cation HFC=C$^+$ (14.30 eV) is calculated to lie above the appearance energy for $m/z = 44$ (14.18 eV) and is therefore not playing any role at the threshold.

The HF loss is the most abundant reaction up to the energetic threshold for F abstraction (formation of $C_2H_2F^+ = m/z$ 45). The fractional abundance of the F abstraction is growing much faster with energy than the HF abstraction as can be expected for a statistical description of a simple bond-breaking reaction. In the energy range, where the parent ion is metastable, fragment ions of mass 45 cannot be distinguished from those of mass 44 in the TOF spectrum. Therefore, we were not able to determine the appearance potential of the F abstraction. The fractional abundance in Figure 3 is referring to both fragments (45 and 44) up to 14.60 eV. The mass 45 is the most abundant species at 17 eV. It might be interesting to note that there is no electronic state coinciding with that energy and therefore isolated state behavior can be ruled out. For energies above 19 eV, the relative abundance of the mass 44 is growing up again, while the relative abundance of mass 45 is decreasing.

The H abstraction (formation of $C_2HF_2^+ = m/z$ 63) is observed ca. 420 meV above the thermochemical threshold and has its maximum in fractional abundance (ca. 30%) at 18.3 eV. It is clearly not metastable in contrast to the results of Jennings.[22] The H loss has also been investigated by Franck[24] by the MIKES technique under collison-free conditions. In that work, the reaction was not found to be metastable.

**TABLE 1: Calculated Thermochemical Thresholds and Experimental Appearance Energies of $C_2H_3F$**

| mass of ion | reaction | thermochemical threshold [eV][b] | experimental AP[a] | this work |
|---|---|---|---|---|
| 46 | fluoroethene $C_2H_3F^+$ | | 10.35 | |
| 45 | $C_2H_3F^+ \rightarrow C_2H_2F^+ + H$ | 13.554 | 13.64 | 13.60 |
| 44 | $\rightarrow C_2HF^+ + H_2$ | 13.803[c] | 13.72 | 13.68 |
| | $\rightarrow HFC{=}C^+ + H_2$ | 14.985 | | |
| 33 | $\rightarrow CH_2F^+ + CH$ | 16.247 | 14.60 | |
| 32 | $\rightarrow CHF^+ + CH_2$ | 17.099 | 17.4 | 20.02 |
| 31 | $\rightarrow CF^+ + CH_3$ | 14.704 | 14.74 | 14.90 |
| 27 | $\rightarrow C_2H_3^+ + F$ | 13.787 | 13.84 | metastable |
| 26 | $\rightarrow C_2H_2^+ + HF$ | 12.377 | 13.51 | 13.41 |
| | $\rightarrow H_2C{=}C^+ + HF$ | ca. 13.51 | | |
| 25 | $\rightarrow C_2H^+ + H + HF$ | 18.421 | 18.23 | 20.02 |
| | $\rightarrow C_2H^+ + H_2 + F$ | 19.808 | | |
| 15 | $\rightarrow CH_3^+ + CF$ | 15.415 | 15.76 | 16.59 |
| 14 | $\rightarrow CH_2^+ + CHF$ | 16.933 | 16.60 | 20.02 |

[a] Kaufel[13] or Reinke et al.[11]   [b] Lias et al.[37] for 0 K   [c] $\Delta H_f$ ($C_2HF^+$) to be corrected.

**TABLE 2: Calculated Thermochemical Thresholds and Experimental Appearance Energies of $C_2H_2F_2$**

| mass of ion | reaction | thermochemical threshold [eV][b] | experimental AP[a] | this work |
|---|---|---|---|---|
| 64 | 1,1-difluoroethene $C_2H_2F_2^+$ | | 10.29 | |
| 63 | $C_2H_2F_2^+ \rightarrow C_2HF_2^+ + H$ | 15.692 | 15.70 | 16.11 |
| 62 | $\rightarrow C_2F_2^+ + H_2$ | 14.98 | | 18.22 |
| | $\rightarrow F_2C{=}C^+ + H_2$ | 15.66 | | |
| 51 | $\rightarrow CHF_2^+ + CH$ | 16.083 | 14.87 | 18.22 |
| 50 | $\rightarrow CF_2^+ + CH_2$ | 16.915 | | 18.22 |
| 45 | $\rightarrow C_2H_2F^+ + F$ | 14.255 | 14.37 | 14.40 |
| 44 | $\rightarrow C_2HF^+ + HF$ | 13.116 | 14.18 | 14.10 |
| | | (12.991[c]) | | |
| | $\rightarrow HFC{=}C^+ + HF$ | 14.30 | | |
| 43 | $\rightarrow C_2F^+ + H + HF$ | | 18.85 | 19.10 |
| | $\rightarrow C_2F^+ + H_2 + F$ | | | |
| 33 | $\rightarrow CH_2F^+ + CF$ | 14.854 | 14.84 | 14.77 |
| 31 | $\rightarrow CF^+ + CH_2F$ | 14.989 | 14.92 | 14.95 |
| 26 | $\rightarrow C_2H_2^+ + F_2$ | 17.339 | 19.08 | 19.15 |
| | $\rightarrow C_2H_2^+ + F + F$ | 18.985 | | |
| | $\rightarrow H_2C{=}C^+ + F_2$ | 18.47 | | |
| 25 | $\rightarrow C_2H^+ + F + HF$ | 19.121 | 19.14 | |
| 14 | $\rightarrow CH_2^+ + CF_2$ | 15.816 | 16.30 | 17.78 |

[a] Kaufel.[13]   [b] Lias et al.[37] for 0 K.   [c] Calculated with a corrected value of $\Delta H_f$ (1181 kJ/mol instead of 1193 kJ/mol).

The ions of mass 33 (formation of $CH_2F^+$) and 31 (formation of $CF^+$) appear at energies 40–80 meV below the thermochemical thresholds, which can be rationalized by thermal energy of the neutral precursor molecules at room temperature. Mass 33 appears at 14.77 eV, and its abundance is growing steeply up to a maximum of over 40% at 15.4 eV. Mass 31 appears at 14.95 eV. Its abundance is growing more slowly and reaches a maximum of ca. 28% at 15.7 eV. Above 15.7 eV, the relative abundance of both mass 33 and 31 is decreasing. The ion of mass 31 is gaining intensity again in the energy range above 19 eV, where it becomes the most abundant fragment with more than 30%. These two reactions are particularly interesting because they lead to very similar species with just the charge being on a different fragment. The relevant transition states and intermediate structures have been calculated for the X state by Frenking et al.[18] One important intermediate seems to be a fluoromethyl carbenium ion ($H_2FC-CF^+$), from which both fragments can be formed. This carbenium ion in turn can be formed from the parent ion by F migration.

An interesting feature of the breakdown diagram in Figure 3 is the dramatic change of fractional abundances in the range between 19 and 19.6 eV. Although there is an electronic state (D) coinciding with that energy it is not very likely that the D state is isolated. The structure in the TPES suggests that the lifetime of this state is larger than $10^{-13}$ s. Most likely, the reactions observed in the region of the D state occur on the electronic ground-state surface of the 1,1-difluoroethene like all the other reactions discussed in this work. A detailed explanation of the change in the breakdown diagram will be given in a later section.

**III.3. Kinetic Energy Distributions.** For the determination of the KER distributions, 10–15 spectra for each molecule have been recorded and analyzed as described before in the energy range up to 20 eV.

*III.3.1. Fluoroethene.* In Figure 4, the TOF spectra and the obtained KER distributions for the HF loss reaction and the F loss reaction of the fluoroethene cation are shown for three energies. The average values for the KER, $\langle KER \rangle$, derived from the full distributions for these reactions are shown in Figure 5.

Just above the appearance energy, the peak of HF loss reaction (at 14.24 eV in Figure 4) has a flat top and is already very broad. The corresponding KER distribution has no contribution from the lower KER values. The width of the peak indicates that the highest possible value for the KER, the excess energy, contributes significantly. For these molecules the entire excess energy is converted to kinetic energy of the fragments. This implies that, besides from the internal energy which stems from the internal energy of the parent, these fragments are rotationally and vibrationally cold. The average value of the KER is more than 1 eV at the threshold for detection (recall that this excitation energy is already lying 1.9 eV above the thermochemical limit). The extracted KERD reveals that a large
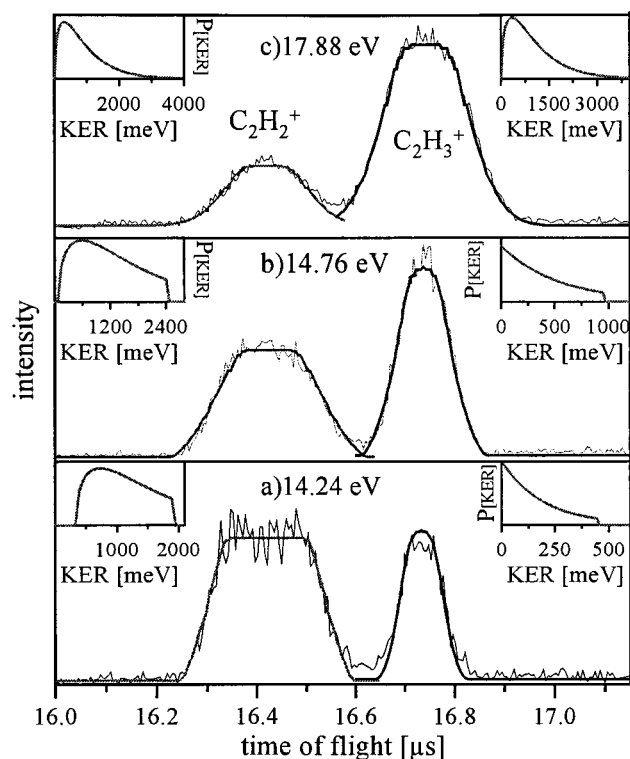
Kinetic Energy Release Distributions

*J. Phys. Chem. A, Vol. 103, No. 42, 1999* **8409**



**Figure 4.** TOF spectra and simulations of the fragments with $m/z =$ 26 (HF loss = $C_2H_2^+$) and 27 (F loss = $C_2H_2F^+$) from fluoroethene at three different excitation energies. The corresponding KER distributions are displayed as inserts (note the different scales of the KER axis).
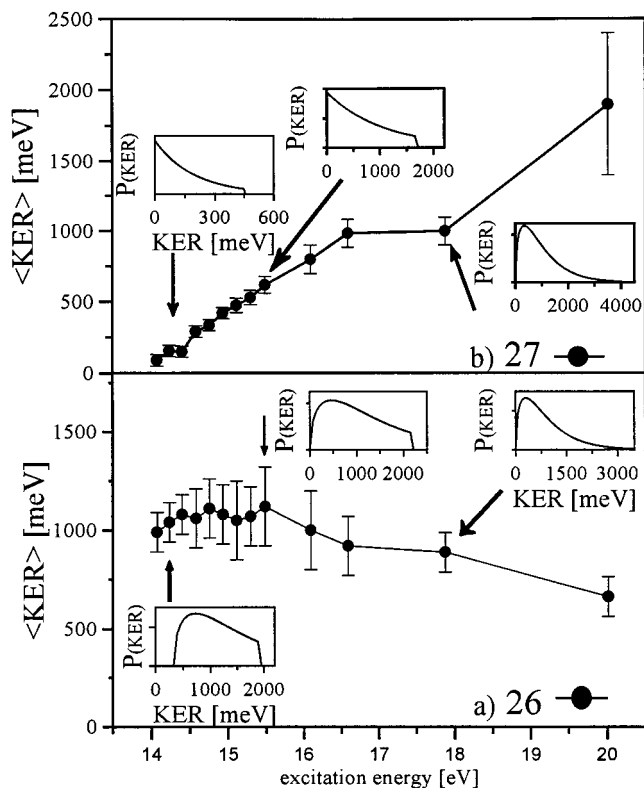


**Figure 5.** Averaged KER ($\langle KER \rangle$) derived from complete KER distributions for the fragments with $m/z =$ 26 and 27 from fluoroethene. The inserts represent KER distributions for the excitation energies indicated.

part of the reverse barrier for this reaction is directly converted into kinetic energy of the products, while the reaction takes place. In this case, the effective height of the reverse barrier at

that internal energy can be directly seen from the KERD to be on the order of 350 meV. At 14.24 eV, the peak of the F loss reaction is almost Gaussian and the KER can be described by a thermal distribution. At an excitation energy only 520 meV higher (Figure 4b), this behavior is already less pronounced. The peak of the F loss reaction is broader and the top of the peak for the HF loss reaction is not so clearly flattened anymore. The KERD for HF loss now reveals a higher distribution of small KER values. At this energy, the barrier is obviously less important and energy randomization can take place between all degrees of freedom in the reacting complex.

At the highest energy (17.88 eV), the shape of the two TOF peaks and corresponding KERD's looks very similar, indicating a reaction highly above the threshold with statistical energy randomization. The average of the kinetic energy is slowly rising for the F loss reaction, as can be expected for a reaction which is statistical. The HF loss reaction is probably also statistical but starts at a value which is determined by the reverse barrier of the reaction. With increasing excitation energy, the average KER for HF loss is in fact decreasing. This indicates changes in the energy redistribution during the fragmentation. Apparently, at higher excitation energy a larger fraction of the excess energy goes into internal degrees of freedom of the products. This correlates with a smaller amount of KER.

A bimodal behavior for the KERD of the F loss from fluoroethene as has been predicted by Roorda, Lorquet, and Lorquet[19] and reported by Locht and Momigny[20] was not observed in our energy-selected experiment at 16.59 eV. We tried to fit the TOF peaks with the KERD that has been used for their surprisal analysis by Momigny and Locht. However, this resulted in TOF peaks which were much too narrow for all energies. The KERD and the $\langle KER \rangle$ of the F loss do not seem to exhibit irregularities in the energy range up to 20 eV. The relatively high fractional abundance of F loss (50%) at 17 eV is not considered to give evidence for isolated state behavior. This relative abundance is comparable to the values just below (27% at 15.49 eV) and above (46% at 17.88 eV) the C state. Thus, we cannot confirm the proposition of two different reaction channels for the C state. We would like to point out that the current experiment has the advantage of dealing with energy-selected ions, in contrast to the retarding field measurements mentioned above.

*III.3.2. 1,1-Difluoroethene.* The time-of-flight spectra of 1,1-difluoroethene in the range of 38.9 and 40 $\mu$s are shown in Figure 6 for three different energies. The shape of the TOF peaks depends strongly on the kinetic energy. At the lower energy (14.95 eV), slightly above the threshold (14.1 eV) of the reaction, the peak shape of the mass 45 (F loss reaction) is close to Gaussian, representing an almost thermal distribution of kinetic energy. The peak of mass 44 (HF loss), however, is much broader and exhibits a flat top. The corresponding KERD ranges from 350 meV to the highest energy possible at that ion internal energy (the excess energy). The flattened top can only be reproduced by simulation if the low KER values <350 meV do not contribute to the fragmentation. This agrees very well with the fact that the calculated[18] transition state ($\approx$15.5 eV) lies above the appearance energy. At this energy, the reaction has to proceed by tunneling of H atoms through the barrier of the transition state and the excess energy of the barrier will not be distributed among all degrees of freedom. Here, a major part of the reverse barrier will be directly converted to translational energy of the fragments.

At 15.71 eV, the HF loss appears to be closer to the statistical case. This excitation energy is almost identical to the height of
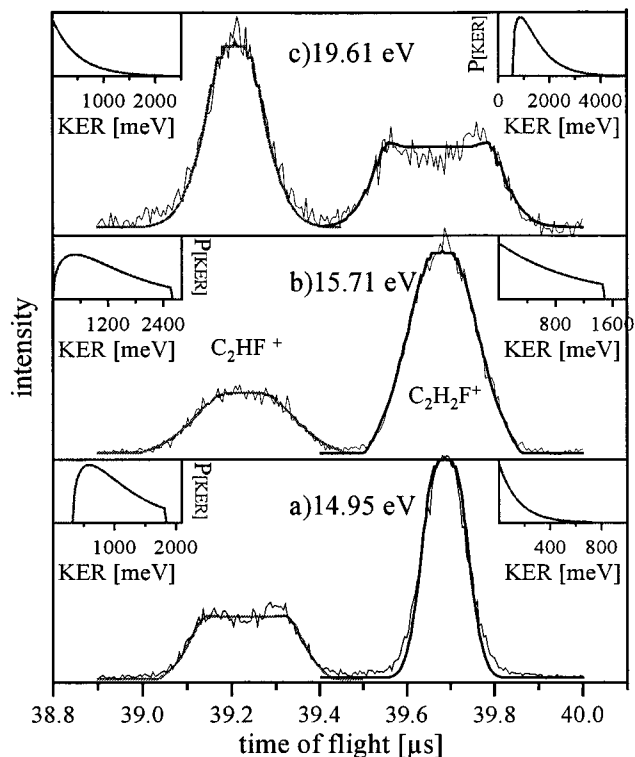
**Figure 6.** TOF spectra and simulations of the fragments with $m/z =$ 44 (HF loss = $C_2HF^+$) and 45 (F loss = $C_2H_2F^+$) from 1,1-difluoroethene at three different excitation energies. The corresponding KER distributions are displayed as inserts (note the different scales of the KER axis).



**Figure 7.** Averaged KER ($\langle KER \rangle$) derived from complete KER distributions for the fragments with $m/z = 44$ and 45 from 1,1-difluoroethene. The inserts represent KER distributions for the excitation energies indicated. Note that the averaged KER is clearly decreasing with increasing energy for mass 44.



**Figure 8.** Averaged KER ($\langle KER \rangle$) derived from complete KER distributions for the fragments with $m/z = 33$ and 31. For comparison the $\langle KER \rangle$ curve as expected for a statistical reaction is presented.

the calculated transition state, and therefore the transition state should have less effect on the energy distribution during the reaction. The peak of the F loss reaction is becoming much broader with increasing energy but still can be described by a KERD for a statistical reaction.

At 19.61 eV, the situation is different. Here, the TOF peak for the HF loss reaction exhibits a Gaussian shape and that for the F loss reaction has a flat top and almost rectangular shape. This peak can only be fitted when KER values up to 550 meV are omitted from the simulation. The KERD in Figure 6c shows that very high KER values contribute to the peak. This behavior cannot be explained by a barrier as for Figure 6a except under the assumption that the reaction is taking place on the energy surface of an excited isolated state (for example the D state which starts at around 19 eV). However, this does not seem to be the case. An alternative explanation will be given at the end of this section.

The average of the KER, $\langle KER \rangle$, of the F loss reaction is increasing with the energy as can be seen in Figure 7b. This is different for the HF loss (Figure 7a), where $\langle KER \rangle$ is almost constant over an energy range of 3.5 eV and is actually decreasing for higher energies.

The dependence of the $\langle KER \rangle$ on the excitation energy for the reactions leading to the fragments with ions of mass 33 and 31 is shown in Figure 8. The absolute value for $\langle KER \rangle$ is much lower than for all the other reactions presented above and lie between 0 and 300 meV. The range of these values agrees well with the MIKES experiments that have been performed on this molecule.[38] The shape of the TOF peaks of mass 31 and 33 is Gaussian for all spectra in the energy range examined. The $\langle KER \rangle$ shows a weak dependence on the excitation energy that is not far from the dependence of a statistical theory. To get an estimate of the theoretically expected $\langle KER \rangle$, the formula given

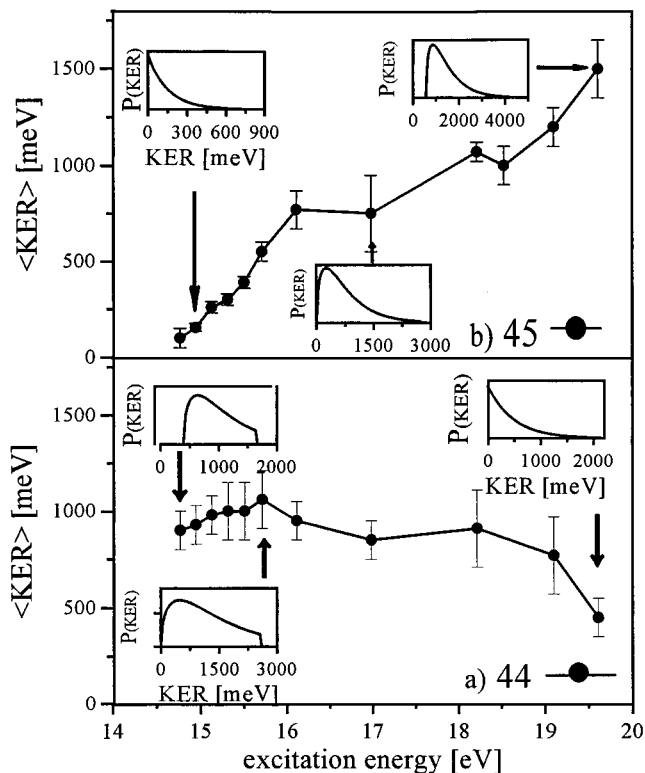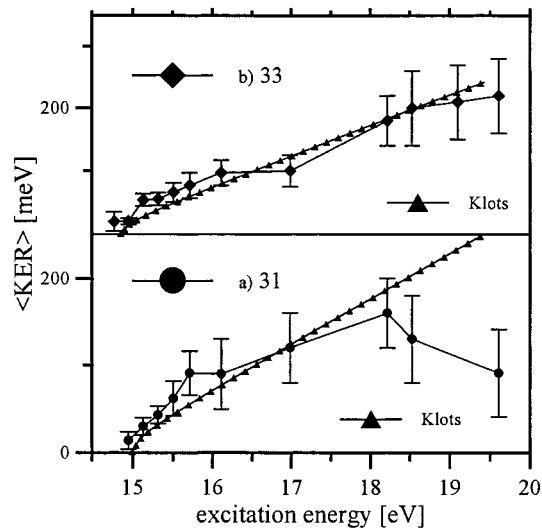by Klots for statistical reactions has been employed.[39] The original formula includes the vibrational frequencies of the products. Only a few of the frequencies of the $CFH_2^+/CF$ and the $CF^+/CH_2F$ ions/neutrals are known.[40,41] These lie between 997 and 1279 $cm^{-1}$. To get at least a qualitative picture, we decided to make a crude approximation by assuming all seven frequencies to be 1000 $cm^{-1}$. The result of this calculation is shown for comparison in Figure 8 as small triangles. The statistical approach seems to fit the experiment quite well for mass 33 and for mass 31 up to 18 eV. Toward higher energies, the $\langle KER \rangle$ for mass 31 is also decreasing. The similarity in the

Kinetic Energy Release Distributions

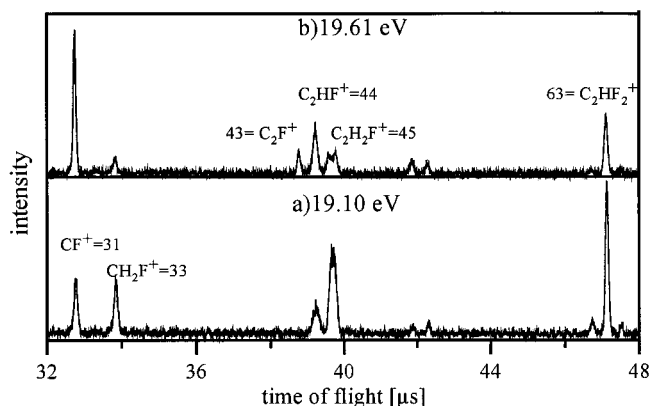*J. Phys. Chem. A, Vol. 103, No. 42, 1999* **8411**



**Figure 9.** Two TOF spectra at energies indicated, which are only 510 meV apart. Note the drastic change of relative intensities. Two fragments with $m/z = 14$ and 26 are not shown in this spectrum but gain also in intensity.

**TABLE 3: Calculated Thermochemical Thresholds of the Energetically Lowest Consecutive Reactions of $C_2H_2F_2$ According to Ref 37**

| reaction | thermochemical threshold (eV) |
|---|---|
| $C_2H_2F_2^+ \rightarrow C_2H_2F^+ (45) + F \rightarrow C_2H_2^+ (26) + F + F$ | 18.99 |
| $C_2H_2F_2^+ \rightarrow C_2H_2F^+ (45) + F \rightarrow C_2HF^+ (44) + H + F$ | 18.89 |
| $C_2H_2F_2^+ \rightarrow C_2HF_2^+ (63) + H \rightarrow C_2HF^+ (44) + F + H$ | 18.89 |
| $C_2H_2F_2^+ \rightarrow C_2H_2F^+ (45) + F \rightarrow CF^+ (31) + CH_2 + F$ | 20.20 |
| $C_2H_2F_2^+ \rightarrow C_2HF_2^+ (63) + H \rightarrow CF^+ (31) + CHF + H$ | 18.72 |
| $C_2H_2F_2^+ \rightarrow C_2HF^+ (44) + HF \rightarrow CF^+ (31) + CH + HF$ | 18.68 |
| $C_2H_2F_2^+ \rightarrow CH_2F^+ (33) + CF \rightarrow CF^+ (31) + H_2 + CF$ | 15.06 |
| $C_2H_2F_2^+ \rightarrow C_2H_2F^+ (45) + F \rightarrow CH_2^+ (14) + CF + F$ | 21.40 |

behavior of the fragments 31 and 33 up to about 18 eV can be explained by the crossing of the potential energy curves mentioned above.[21] Since this crossing is supposed to occur late on the reaction coordinate, the two reaction channels behave similarly and the site of the charge is decided at a point, where the fragmentation of the molecule is almost complete.

**III.4. Consecutive Reactions in the 1,1-Difluoroethene.** As has been pointed out above, the fragmentation behavior of 1,1-difluoroethene changes dramatically at energies between 19 and 20 eV. The three most important aspects are listed below.

(i) The breakdown diagram shows a steep decrease for the fragments 45 and 63 and a steep increase for fragment 31 and 44.

(ii) The average values $\langle KER \rangle$ for the fragments 44 and 31 seem to decrease with increasing energy.

(iii) The TOF peak of the fragment 45 exhibits a flat top resulting from a change in KER distribution, where low KER values are not represented. The TOF peaks of the fragments 44 and 31 become narrower due to a higher contribution of small KER values.

For a further illustration, two TOF spectra taken at energies only ca. 500 meV apart are shown in Figure 9. The features listed above can all be explained consistently by considering consecutive reactions. Consecutive reactions occur if the energy stored in the internal degrees of freedom of the fragments is above the threshold for further fragmentation. The thermochemical thresholds for eight of these consecutive reactions are shown in Table 3. At least six of these reaction channels are open at energies above 19 eV. The fragment 45, e.g., can further react by F loss and H loss to the fragments 26 and 44, while fragment 63 can react by F loss and CHF loss to the fragments 44 and 31. The fragments 44 and 33 can also be depleted by reaction channels leading to fragment 31. These considerations explain the change in the branching ratios mentioned earlier.

The fractional abundance of fragment 44 is affected the least because it is gaining intensity from some channels and loosing intensity to others.

Looking at the KER data, this assignment is getting even more convincing due to the following reasoning. It can be assumed that the reactions leading to the primary fragments follow a statistical mechanism. In that case, the reaction takes place by distributing the excess energy among the internal degrees of freedom of the fragments and the translational energy, which is observable as KER. Primary fragments with high internal energy will undergo consecutive reactions if they are energetically accessible. Fragments which are formed in such a consecutive reaction are expected to form narrower mass peaks and have smaller $\langle KER \rangle$ at the threshold of the reaction, because a large share of the energy is used to break bonds and not much is left for KER. This is the case for the masses 31 and 44. On the other hand, primary fragments that are subject to further fragmentation are expected to form broader peaks and have a steeply increasing $\langle KER \rangle$, because only these ions are reactive that have high internal energy and therefore low KER. These ions are depleted in the KERD leaving only the internally less energized ions with high KER. This effect can be nicely visualized by examining Figure 10. The peak of mass 45 seems to be reduced by only the narrow top corresponding to the low KER in the KERD and to internally energized (therefore reactive) part of the ions. On the other hand, peak 45 seems to gain only a narrow top from consecutive reactions, corresponding to ions which cannot have a high KER value for energetic reasons. This discussion demonstrates that the analysis of the KER distribution of energy-selected ions opens access to new information regarding the mechanism which is difficult to obtain otherwise.

Combining the information from branching ratios, thermochemical calculations, and KER analysis the reactions between 19 and 20 eV can now be explained by consecutive reactions as schematically shown below:
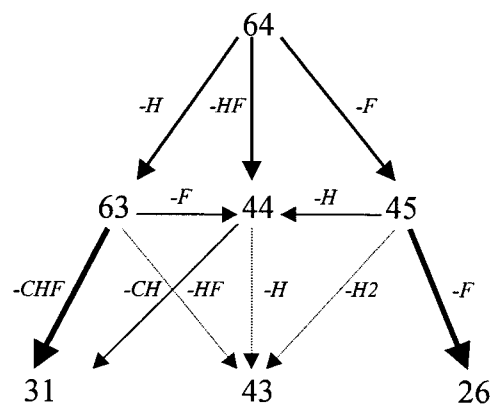


(i) Intensity of mass 45 is decreased due to further reaction to 26 (F loss, major) and 44 (H loss, minor).

(ii) Intensity of mass 63 is decreased due to further reaction to 31 (CHF loss, major) and 44 (F loss, minor).

(iii) Intensity of mass 44 is increased due to reaction of 63 (F loss) and 45 (H loss) and decreased due to further reaction to 31 (CH loss, major) and 43 (H loss, minor).

(iv) Intensity of mass 26 is increased due to reaction of 45 (F loss) exclusively.

(v) Intensity of mass 31 gains the most by reaction of 44 (CH loss) and 63 (CHF loss).

(vi) Intensity of mass 43 can be increased by reactions of all possible precursors 63 (HF loss), 45 (F loss), and 44 (H loss) and is only a minor peak in the mass spectrum.
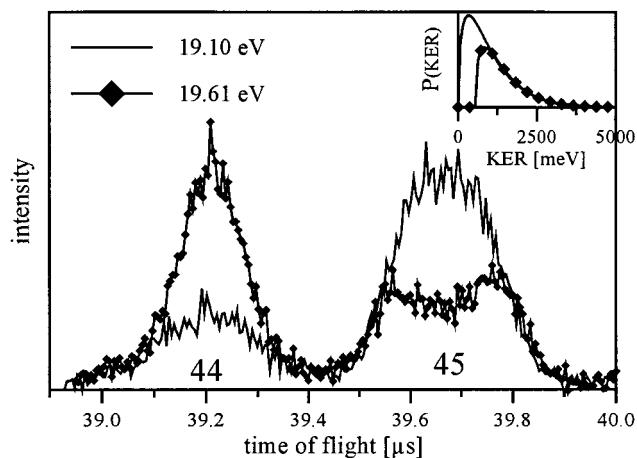
**Figure 10.** The two TOF spectra from Figure 9 plotted together in the TOF range of the fragments with $m/z = 44$ and 45. The insert shows the KERD for fragment 45.

The enhanced production of the $CH_2^+$ fragment ($m/z = 14$) at high energies can, however, not be explained by consecutive reactions because the threshold for the only possible channel is too high. This fragment is formed by direct cleavage of the C=C double bond. Its intensity is probably slowly rising with energy due to steric reasons.

For the fragment $C_2H_2^+$ ($m/z = 26$), the formation of $F_2$ is unlikely compared to two consecutive F loss reactions. It is energetically possible that the $C_2H_2F^+$ ion rearranges prior to further reaction. This explanation is also in agreement with the measured appearance energies. One should point out that all reactions (including consecutive reactions) for which a KER analysis has been performed in this work are relatively fast ($k > 10^7$ s$^{-1}$). Otherwise, the TOF peaks would be asymmetrical. Note, however, that the metastable energy range will be discussed elsewhere.

## IV. Summary

The unimolecular reactions of energy-selected fluoroethene and 1,1-difluoroethene ions have been investigated in the energy range between 13 and 20 eV. The variation of the relative abundance's of fragment ions has been discussed. For the most important reactions, complete kinetic energy release distributions were derived from a direct simulation of the experimental coincidence TOF spectra. Some of the product kinetic energy distributions are highly nonthermal due to a barrier for the reverse reaction. A particularly interesting switching in the KERD is observed for the HF and F loss reaction from 1,1-difluoroethene. At low excitation energies, the KERD for the HF loss is nonthermal, while that for F loss is thermal. At high excitation energy this is reversed. There the F loss is nonthermal and the HF loss is thermal. The kinetics of the HF loss reaction from fluoroethene and 1,1-difluoroethene ions will be described in a forthcoming paper. The role of consecutive reactions in the 1,1-difluoroethene ion has been evidenced from the analysis of TOF distributions and KERD distributions.

## References and Notes

(1) Bralsford, R.; Harris, P. V.; Price, W. C. *Proc. R. Soc. (London)* **1960**, *A258*, 459.

(2) Lake, R. F.; Thompson, H. *Proc. R. Soc. (London)* **1970**, *A315*, 323.

(3) Turner, T. A.; Baker, C.; Baker, A. D.; Brundle, C. R. *Molecular Photoelectron Spectroscopy*; Wiley & Sons: London, 1970.

(4) Sell, A.; Kuppermann, A. *J. Chem. Phys.* **1979**, *71*, 4703.

(5) Bieri, G.; von Niessen, W.; Åbrink, L.; Svensson, A. *Chem. Phys.* **1981**, *60*, 61.

(6) Bieri, G.; Åbrink, L.; von Niessen, W. *J. Electron. Spectrosc. Relat. Phenom.* **1981**, *23*, 281.

(7) Leyh, B.; Locht, R.; Hottmann, K.; Baumgärtel, H. *BESSY-Jahresbericht* **1995**, 163.

(8) Lifshitz, C.; Long, F. A. *J. Phys. Chem.* **1963**, *67*, 2463.

(9) Lifshitz, C.; Long, F. A. *J. Phys. Chem.* **1965**, *69*, 3731.

(10) Lifshitz, C.; Long, F. A. *J. Phys. Chem.* **1965**, *69*, 3737.

(11) Reinke, D.; Krässig, R.; Baumgärtel, H. *Z. Naturforsch., Teil A* **1973**, *28*, 1021.

(12) Reinke, D.; Baumgärtel, H.; Cvitaš, T.; Klasinc, L.; Güsten, H. *Ber. Bunsen-Ges. Phys. Chem.* **1974**, *78*, 1145.

(13) Kaufel, R. Dissertation, Freie Universität Berlin, 1985.

(14) Ibuki, T.; Imamura, T.; Koyano, I.; Masuoka, T.; Brion, C. E. *J. Chem. Phys.* **1993**, *98*, 2908.

(15) Dannacher, J.; Schmelzer, A.; Stadelmann, J. P.; Vogt, J. *Int. J. Mass Spectrom. Ion Phys.* **1980**, *31*, 175.

(16) Frey, R. Dissertation, Universität Freiburg, 1974.

(17) Stadelmann, J. P.; Vogt, J. *Int. J. Mass Spectrom. Ion Phys.* **1980**, *35*, 83.

(18) Frenking, G.; Koch, W.; Schaale, M.; Baumgärtel, H. *Int. J. Mass Spectrom. Ion Processes* **1984**, *61*, 305.

(19) Roorda, M.; Lorquet, A. J.; Lorquet, J. C. *J. Phys. Chem.* **1991**, *95*, 9118.

(20) Momigny, J.; Locht, R. *Chem. Phys. Lett.* **1993**, *211*, 161.

(21) Lorquet, J. C. In *The Structure, Energetics and Dynamics of Organic Ions*; Baer, T., Ng, C. Y., Powis, I., Eds.; Wiley: New York, 1996.

(22) Jennings, K. R. *Org. Mass Spectrom.* **1969**, *3*, 85.

(23) Cooks, R. G.; Kim, K. C.; Beynon, J. H. *Int. J. Mass Spectrom. Ion Phys.* **1974**, *15*, 245.

(24) Franck, B. Diploma thesis, Université de Liège, 1996.

(25) Kim, K. C. *J. Chem. Phys.* **1976**, *64*, 3003.

(26) Baer, T. In *Gas-Phase Ion Chemistry*; Bowers, M. T., Ed.; Academic Press: New York, 1979; Vol. 1.

(27) Baer, T.; Booze, J.; Weitzel, K.-M. In *Vacuum Ultraviolet Ionisation and Dissociation of Molecules and Clusters*; Ng, C. Y., Ed.; World Scientific Publishing Co.: Singapore, 1991.

(28) Güthe, F.; Malow, M.; Weitzel, K.-M.; Baumgärtel, H. *Int. J. Mass Spectrom. Ion Processes* **1998**, *172*, 47.

(29) Güthe, F. Dissertation, Freie Universität Berlin, 1997.

(30) Güthe, F.; Weitzel, K.-M. To be published.

(31) Stockbauer, R. *Int. J. Mass Spectrom. Ion Phys.* **1977**, *25*, 89.

(32) Mintz, D. M.; Baer, T. *J. Chem. Phys.* **1976**, *65*, 2407.

(33) Powis, I.; Mansell, P. I.; Danby, C. J. *Int. J. Mass Spectrom. Ion Processes* **1979**, *31*, 15.

(34) Franklin, J. L.; Hierl, P. M.; Whan, D. A. *J. Chem. Phys.* **1967**, *47*, 3148.

(35) Weitzel, K.-M.; Güthe, F.; Mähnert, J.; Locht, R.; Baumgärtel, H. *Chem. Phys.* **1995**, *287*, 201.

(36) Momigny, J. In *Gaseous Molecular Ions*; Baumgärtel, H., Franck, E. U., Grünbein, W., Eds.; Steinkopff Verlag: Darmstadt, 1992.

(37) Lias, S. G.; Bartmess, J. E.; Liebman, J. F.; Holmes, J. L.; Levin, R. D.; Mallard, W. G. *J. Phys. Chem. Ref. Data* **1988**, *17* (Suppl. 1).

(38) Leyh, B. Unpublished results.

(39) Klots, C. E. *J. Chem. Phys.* **1973**, *58*, 5364.

(40) Jacox, M. E.; Milligan, D. E. *J. Chem. Phys.* **1969**, *50*, 3152.

(41) Raymond, J. I.; Andrews, L. *J. Phys. Chem.* **1971**, *75*, 3237.